GRAPHICAL PROGNOSIS INCLUDING EFFECTS OF VERTICAL MOTION DUE TO TERRAIN GRADIENTS

Theodore S. Hesse

62

GRAPHICAL PROGNOSIS INCLUDING EFFECTS OF VERTICAL MOTION DUE TO TERRAIN GRADIENTS

* * * * *

Theodore S. Hesse

GRAPHICAL PROGNOSIS INCLUDING EFFECTS OF VERTICAL MOTION DUE TO TERRAIN GRADIENTS

by

Theodore S. Hesse

Lieutenant, United States Navy

Submitted in partial fulfillment of
the requirements for the degree of

MASTER OF SCIENCE
IN
AEROLOGY

United States Naval Postgraduate School
Monterey, California

1957

GRAPHICAL PROGNOSIS INCLUDING EFFECTS OF VERTICAL MOTION DUE TO TERRAIN GRADIENTS

by

Theodore S. Hesse

This work is accepted as fulfilling
the thesis requirements for the degree of
MASTER OF SCIENCE
IN
AEROLOGY

from the
United States Naval Postgraduate School

ABSTRACT

Two prediction models for graphical prognosis are developed and evaluated. The primary feature of these models which represents a departure from previous graphical methods is the inclusion of the terrain-induced vertical velocities. These vertical motions may in turn produce vorticity changes, and thus height changes.

The first model presented is comprised of two separate parts; the first part is a prediction of the 500-mb surface and the second part a prediction of the 1000-mb to 500-mb thickness. The two parts may be combined to produce a surface (1000-mb) prognosis. This model failed to produce satisfactory results, and hence a second model was developed.

The second model presented follows somewhat the development of the first, but avoids an assumption relating the surface and 500-mb winds that is believed to have contributed largely to the original failure. This model operates on the current 1000-mb and 1000-mb to 500-mb thickness charts; and, utilizing a fraction of the 500-mb height change as predicted by any other established method, produces a surface (1000-mb) prognosis. The model was tested in two ways; one with the terrain factor included in the prediction equation and one omitting the terrain factor. Both methods produced satisfactory prognoses. However, inclusion of the terrain factor consistently produced the better results.

The writer wishes to express his appreciation for the assistance and guidance of Professor George J. Haltiner of the U. S. Naval Postgraduate School in the preparation of this paper.

PREFACE

Graphical methods of numerical prognosis have recently received widespread attention since the development by Fjortoft [1] of a prediction model for the 500-mb surface. Fjortoft provided a graphical technique for integration of the barotropic vorticity equation. Despite the relative simplicity of the method and the rather restrictive assumptions inherent in its development, tests by the Air Weather Service of the United States Air Force [2] indicate accuracy comparable to that achieved by a trained forecaster using conventional techniques.

Following the success of Fjortoft's model, several other more involved graphical models have recently been devised. Although none as yet have been subjected to the degree of testing that Fjortoft's model has, preliminary results are encouraging.

The graphical methods devised thus far appear to have been least successful in mountainous terrain areas. The reason for this probably lies in the simplified boundary condition, $\omega = 0$ at p_o, which has been assumed in the previous models.

It is the purpose of this paper to attempt to incorporate terrain effects into graphical techniques of prognosis. The development here is somewhat similar to the treatments of Estoque [3] and Reed [4] .

TABLE OF SYMBOLS AND NOTATION

p	pressure
p_o	1000-mb pressure
p_5	500-mb pressure
t	time
g	acceleration of gravity
ρ_o	density of air at 1000mbs
f	coriolis parameter: $2\Omega \sin \varphi$
Ω	angular velocity of earth's rotation
φ	latitude
d	grid distance for computation of space mean values
m	map scale factor
ω	$\frac{dp}{dt}$, proportional to vertical velocity
σ	$\frac{1}{\theta g \rho} \frac{\partial \theta}{\partial p}$
θ	potential temperature
ζ	relative vorticity
ζ_a	absolute vorticity
Z	height of 500-mb surface
$\overline{Z}$	space-mean height of 500-mb surface
Z_o	height of 1000-mb surface
$\overline{Z}_o$	space-mean height of 1000-mb surface
h	1000- to 500-mb thickness
$\overline{h}$	space-mean 1000- to 500-mb thickness
$\overline{x}$	mean value of quantity x
$\underset{\sim}{Y}$	notation for vector Y
$\underset{\sim}{V}$	500-mb wind

$\underset{\sim}{V}_S$ surface wind

$\underset{\sim}{V}_T$ thermal wind between 1000- and 500mbs

$\underset{\sim}{V}_o$ 1000-mb wind

$\underset{\sim}{\nabla}$ horizontal del operator, $\underset{\sim}{i}\frac{\partial}{\partial x}+\underset{\sim}{j}\frac{\partial}{\partial y}$ on (x,y,p,t) coordinates

H height of surface of ground above sea level in feet

TABLE OF CONTENTS

LIST OF ILLUSTRATIONS

CHAPTER I

FIRST PREDICTION MODEL

The first model is comprised of two parts; the prognosis of the 500-mb surface and a separate prognosis of the 1000-mb to 500-mb thickness. The two prognoses may be combined for a resultant surface (1000-mb) prognosis. The development here parallels that of Estoque [3].

1. Development of the prediction equation for the 500-mb surface.

The "vertical velocity" is assumed to vary thusly:

$$\omega(x,y,p,t) = -Kg\rho_0\left(\underset{\sim}{V}_s \cdot \underset{\sim}{\nabla} H\right)\left(\frac{p}{p_0}\right) + \omega_m(x,y,t)\left[1-\left(\frac{p-p_5}{p_0-p_5}\right)^2\right]. \quad (1)$$

The first term on the right represents the contribution due to the orographic effect and is assumed to vary linearly with pressure (p/p_0), from a maximum at p_0 to zero at the top of the atmosphere. k is a scalar multiplier with possible values ranging between zero and unity. It is assumed to equal unity for this development and hence will not appear in subsequent equations in this chapter. The second term on the right is the contribution due to the non-orographic effects, and is assumed to vary parabolically from zero at $p=p_0$ to a maximum of ω_m at $p=p_5$. Inherent in this distribution is the assumption that p_5 (to be taken as 500mbs) is a level of non-divergence where there are no orographic effects. The non-orographic contribution assumed here varies slightly from Estoque's assumption of a sinusoidal variation of vertical velocity [3].

Differentiating (1) with respect to pressure yields

$$\frac{\partial \omega}{\partial p} = -\frac{g\rho_0}{p_0}\left(\underset{\sim}{V}_s \cdot \underset{\sim}{\nabla} H\right) - 2\omega_m \frac{p-p_5}{(p_0-p_5)^2}. \quad (2)$$

Evaluating (2) at p_5 gives

$$\left(\frac{\partial \omega}{\partial p}\right)_{p_5} = -\frac{g\rho_0}{p_0}\left(\underset{\sim}{V}_s \cdot \underset{\sim}{\nabla} H\right) \tag{3}$$

The following form of the vorticity equation is assumed:

$$\frac{\partial \eta}{\partial t} + \underset{\sim}{V}\cdot\underset{\sim}{\nabla}\eta_a = -f\frac{\partial \omega}{\partial p} \tag{4}$$

This form of the vorticity equation neglects the vertical advection of vorticity, the vortex tube term, and $\eta \partial\omega/\partial p$. Since $\partial\omega/\partial p = -\underset{\sim}{\nabla}\cdot\underset{\sim}{V}$, Eq. (3) shows that the only divergence considered at 500mbs is due to terrain-induced vertical velocities.

Combining (3) and (4) yields

$$\frac{\partial \eta}{\partial t} + \underset{\sim}{V}\cdot\underset{\sim}{\nabla}\eta_a = -\frac{fg\rho_0}{p_0}\underset{\sim}{V}_s\cdot\underset{\sim}{\nabla} H \quad . \tag{5}$$

In order to obtain conservation equations utilizing only 500-mb data, the surface wind must be eliminated from Eq. (5). This will be done by assuming that $\underset{\sim}{V}_s = a\underset{\sim}{V}$, where a is a scalar multiplier. Then (5) may be written

$$\frac{\partial \eta}{\partial t} + \underset{\sim}{V}\cdot\underset{\sim}{\nabla}\eta_a = -\frac{afg\rho_0}{p_0}\underset{\sim}{V}\cdot\underset{\sim}{\nabla} H \quad . \tag{6}$$

Taking mean values of f and ρ_0 for the area to be prognosticated, (6) may be written

$$\frac{\partial \eta}{\partial t} + \underset{\sim}{V}\cdot\underset{\sim}{\nabla}\left(\eta_a + \frac{ag\bar{f}\bar{\rho}_0}{p_0} H\right) = 0 \quad . \tag{7}$$

With the assumption of geostrophic vorticity, this becomes

$$\frac{\partial \eta}{\partial t} + \underset{\sim}{V}\cdot\underset{\sim}{\nabla}\left(\frac{g}{f}\nabla^2 z + f + \frac{ag\bar{f}\bar{\rho}_0}{p_0} H\right) = 0 \quad ; \text{ or}$$

$$\left(\frac{\partial}{\partial t} + \underset{\sim}{V}\cdot\underset{\sim}{\nabla}\right)\left(\frac{g}{f}\underset{\sim}{\nabla}^2 z + f + \frac{ag\bar{f}\bar{\rho}_o}{p_o} H\right) = 0 \qquad (8)$$

as f and $ag\bar{f}\bar{\rho}_o H/p_o$ are invariant with time.

Introducing the finite difference formula for vorticity into Eq. (8) gives

$$\left(\frac{\partial}{\partial t} + \underset{\sim}{V}\cdot\underset{\sim}{\nabla}\right)\left[\frac{4m^2 g}{fd^2}(\bar{z}-z) + f + \frac{ag\bar{f}\bar{\rho}_o}{p_o} H\right] = 0 \qquad (9)$$

Multiplying through by factor $fd^2/4m^2g$, which is invariant with time, and expanding, produces

$$\underset{(a)}{\frac{\partial}{\partial t}\left[(\bar{z}-z) + \underset{(b)}{\frac{f^2 d^2}{4m^2 g}} + \underset{(c)}{\frac{af d^2 \bar{f}\bar{\rho}_o}{4m^2 g p_o}} H\right]} + \underset{(d)}{\underset{\sim}{V}\cdot\frac{fd^2}{4m^2 g}\underset{\sim}{\nabla}\frac{4m^2 g}{fd^2}(\bar{z}-z)} + \underset{\sim}{V}\cdot\frac{fd^2}{4m^2 g}\underset{\sim}{\nabla} f + \underset{\sim}{V}\cdot\frac{fd^2}{4m^2 g}\underset{\sim}{\nabla}\frac{ag\bar{f}\bar{\rho}_o}{p_o} H = 0 \qquad (10)$$

Considering terms of Eq. (10) separately:

(a) This term may be written $\partial/\partial t(\bar{Z} - Z)$, as other terms are invariant with time.

(b) The factor $4m^2g/fd^2$ may be taken outside of $\underset{\sim}{\nabla}$ operator, as variation is small compared with the variation of $(\bar{Z} - Z)$.

(c) Following Fjortoft [1], this term may be written as $\underset{\sim}{V}\cdot\underset{\sim}{\nabla} J(\varphi)$, where

$$J(\varphi) = \int_0^{\varphi} \frac{\Omega^2 d^2 \sin\varphi\cos\varphi}{m^2 g}\, d\varphi$$

(d) Taking mean value of f for area to be prognosticated, this term may be written

$$\underset{\sim}{V}\cdot\underset{\sim}{\nabla}\frac{a\bar{f}^2\bar{\rho}_o d^2}{4m^2 p_o} H$$

Rewriting (10) with above changes gives

$$\frac{\partial}{\partial \tau}(\bar{Z}-Z)+\underset{\sim}{V}\cdot\underset{\sim}{\nabla}\left[(\bar{Z}-Z)+J(\varphi)+\frac{a\bar{f}^{2}\bar{\rho}_{o}d^{2}}{4m^{2}p_{o}}H\right]=0\ . \qquad (11)$$

With the notation

$$B\equiv\frac{a\bar{f}^{2}\bar{\rho}_{o}d^{2}}{4m^{2}p_{o}}H\ ,$$

Eq. (11) becomes

$$\frac{\partial}{\partial \tau}(\bar{Z}-Z)+\underset{\sim}{V}\cdot\underset{\sim}{\nabla}\left[\bar{Z}-Z+J(\varphi)+B\right]=0\ . \qquad (12)$$

As B and $J(\varphi)$ are invariant with time, (12) may be written

$$\frac{\partial}{\partial \tau}\left(\bar{Z}-Z+J(\varphi)+B\right)+\underset{\sim}{V}\cdot\underset{\sim}{\nabla}\left(\bar{Z}-Z+J(\varphi)+B\right)=0 \qquad (13)$$

or, in Jacobian form,

$$\frac{\partial}{\partial \tau}\left(\bar{Z}-Z+J(\varphi)+B\right)+\frac{g}{f}J\left(Z,\ \bar{Z}-Z+J(\varphi)+B\right)=0\ , \qquad (14)$$

which is the desired prediction equation. However, in using the above equation, the advection would be accomplished with the current 500-mb wind, which obviously may vary considerably with time, especially if a prognostic interval of 12 or 24 hours is employed. In order to arrive at an advective field which is more conservative with time, the Jacobian identity $J(X,Y)\equiv J(X+Y,\ Y)$ may be employed. Applying this to (14) gives

$$\frac{\partial}{\partial \tau}\left(\bar{Z}-Z+J(\varphi)+B\right)+\frac{g}{f}J\left(\bar{Z}+J(\varphi)+B,\ \bar{Z}-Z+J(\varphi)+B\right)=0. \qquad (15)$$

Thus the advection is accomplished with a much more conservative field, $(Z+J(\varphi)+B)$, $\bar{Z}$ being the only quantity that varies with time, and this much more slowly than Z.

As a preliminary test of results of the model developed herein,

Fig. 1 was prepared. An initial west-east zonal flow of 50 knots was assumed at 500mbs. The surface wind was assumed to be equal in direction and $\frac{1}{2}$ the magnitude of the 500-mb wind (i.e.; $a = \frac{1}{2}$). Eq. (15) was used and a prognostic chart for a time of six hours was prepared, using height changes as approximated by the first term of Fjortoft's series [1]. The resultant prognostic chart shows a trough in the lee of the Rocky Mountains, as would be expected under the circumstances.

2. Testing of the prediction equation for the 500-mb surface.

The first step in the employment of Eq. (15) was the construction of the $\overline{Z}$ chart. This chart was prepared by conventional graphical methods, using a grid distance d of 10^3km as suggested by Estoque [3]. Next, the contours of $J(\varphi)$ corresponding to a grid distance of 10^3km were added graphically to the $\overline{Z}$ chart. Assuming a value of $\frac{1}{2}$ for a, the quantity B was evaluated as 1.5×10^{-2}, assuming standard values of the meteorological parameters, neglecting variations of m^2, and taking d as 10^3km, as above. (Variations of m^2 are small, as a conformal projection with standard latitudes of 30N and 60N was used, and prognostication was confined to middle latitudes). A terrain contour chart of North America was multiplied by the above constant and isolines of the quantity B were drawn. The B chart was then added to the $\overline{Z} + J(\varphi)$ chart to produce the advective field $(\overline{Z} + J(\varphi) + B)$. The Z chart was then subtracted from the advective field to produce the $(\overline{Z} - Z + J(\varphi) + B)$ field, or the conserved quantity to be advected.

The above two charts were superimposed in register, and isolines of $(\overline{Z} - Z + J(\varphi) + B)$ advected geostrophically with the $(\overline{Z} + J(\varphi) + B)$ chart for the chosen prognostic interval of 12 hours.

Fig. 1

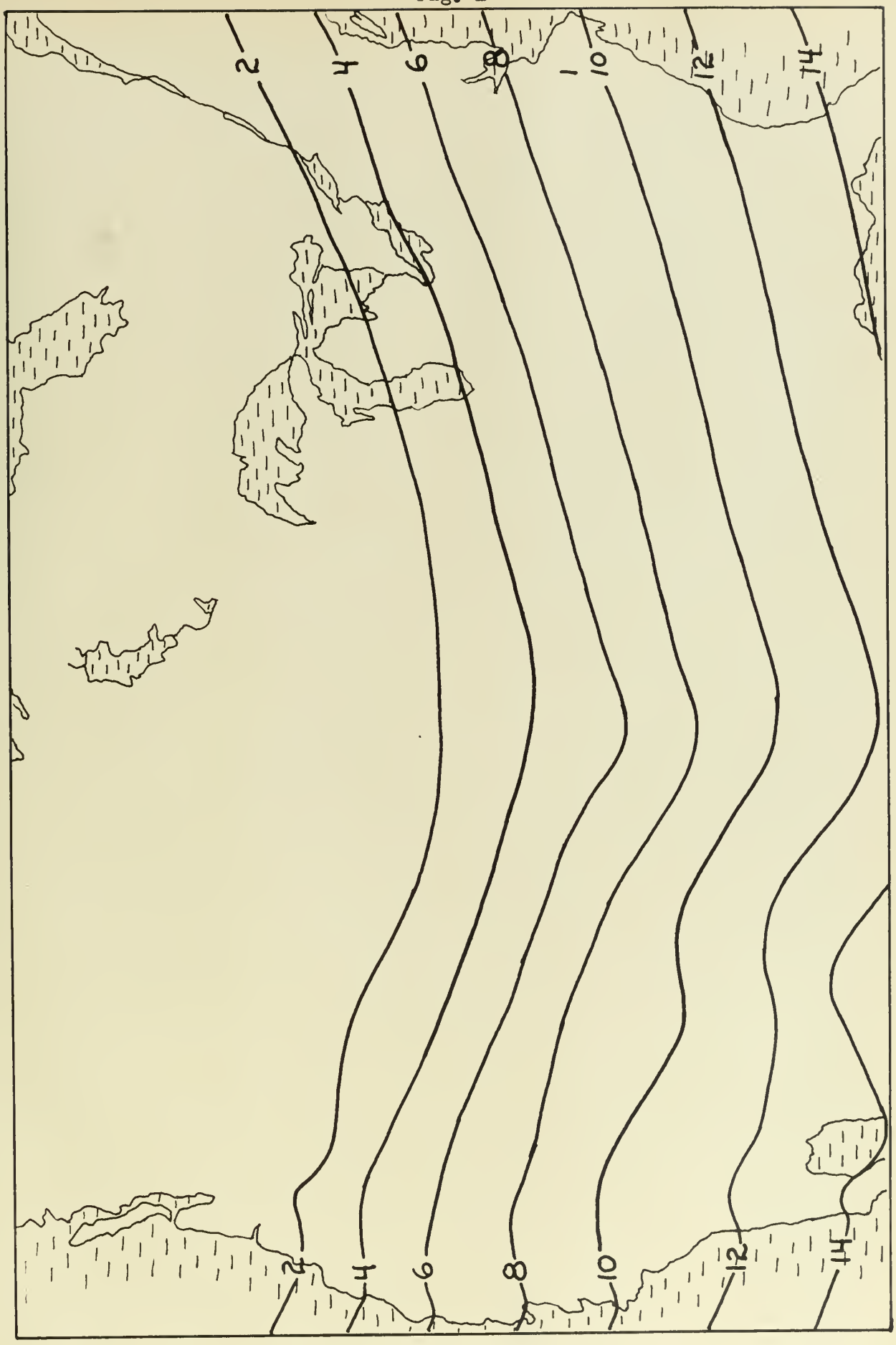

The prognostic 12-hr height changes may have been recovered by use of Fjortoft's series [1],

$$\Delta Z = \Delta\left(\bar{Z} - Z + J(\varphi) + B\right) + \overline{2\left(\bar{Z} - Z + J(\varphi) + B\right)}$$

and compared with observed values of height changes, but for this test a more direct method of evaluation was used. The quantity $(\bar{Z} - Z + J(\varphi) + B)$ was advected for the 12-hr period and compared with the observed values of the same quantity as computed from the observed chart at the end of the prognostic period.

The results of four tests using the above techniques and assumptions were generally poor. Indications were that in some isolated regions the inclusion of the terrain factor gave better results than the use of the prediction equation

$$\frac{\partial}{\partial t}\left(\bar{Z} - Z + J(\varphi)\right) + \frac{g}{f} J\left(\bar{Z} + J(\varphi), \bar{Z} - Z + J(\varphi)\right) = 0. \quad (16)$$

(Except for the different vertical velocity distribution assumed, this equation is essentially the same as Estoque's model [3]). However, these regions of improved results were not constant in space nor were they predictable, and the areas of poorer results generally equalled or exceeded the improved regions, resulting in generally poorer prognoses by inclusion of the terrain factor than by ignoring it.

It was reasoned that the choice of $a = \frac{1}{2}$, i.e., that the surface wind is equal in direction and $\frac{1}{2}$ the magnitude of the 500-mb wind (in connection with the terrain factor), may have been largely responsible for the failure of the method. Therefore, another technique was developed using a equal to either $\frac{1}{2}$, zero, or $-\frac{1}{2}$, as determined in the following manner. The current 500-mb and 850-mb charts were superimposed, and areas delineated where the 500-mb contours were approximately the same

direction as, at right angles to, or opposite in direction to the 850-mb contours. The 850-mb chart was selected as the chart most nearly representing the surface in the majority of the mountainous areas. Then, in producing the $(\overline{Z} + J(\varphi) + B)$ chart, the contours of B as drawn for the first technique were added, considered zero, or subtracted in the areas indicated. The subsequent steps in this technique were as before.

Results of using the new technique were slightly better than for the assumption that a is everywhere $\frac{1}{2}$. However, improvements realized were insufficient to justify use of the method. A prime difficulty in application was the determination of appropriate values of a, which appeared to vary rapidly over small areas, especially in situations where closed lows were present at the 500-mb or 850-mb levels. An extensive search was made to locate a synoptic situation where the differences between 500-mb and 850-mb wind fields were clear-cut, in an attempt to evaluate the technique objectively. Such a situation was located, and results of the testing indicated that whereas the sign of a was correctly chosen by the above technique, the magnitude of a appeared to vary considerably from the assumed values of $\frac{1}{2}$, zero, and $-\frac{1}{2}$. As a consequence, the prognostication was not appreciably better than that using Eq. (16), and indications were that even if the sign of a were predictable, the magnitude would vary to such a degree that prognostications ignoring the terrain factor would be more reliable.

3. Conclusions as to prognosis of the 500-mb surface.

No improvement over Estoque's prediction model [3] is realized by inclusion of terrain effects on vertical motion by methods developed in this paper. It is believed that the major reason for the failure lies in the difficulty of expressing the surface wind in terms of the 500-mb wind

in the 500-mb conservation equation.

4. Development of the prediction equation for the 1000- to 500-mb thickness.

A detailed development of the prediction equation will not be presented here. The development follows closely the methods of Section 1 of this chapter, so a listing of the major assumptions and the final equation will be shown.

Assumptions:

(a) The vertical velocity distribution is as described in Eq. (1).

(b) Temperature changes are adiabatic. The following form of the adiabatic thermal equation is employed:

$$\frac{\partial}{\partial t}\left(\frac{\partial z}{\partial p}\right) + \underset{\sim}{V}\cdot\underset{\sim}{\nabla}\frac{\partial z}{\partial p} + \omega\sigma = 0 \qquad (17)$$

(c) $\underset{\sim}{V}_T \cdot \underset{\sim}{\nabla} z_0$ and $\underset{\sim}{V}_0 \cdot \underset{\sim}{\nabla} f$ are relatively small and are neglected.

(d) Similar assumptions as those used in progressing from Eq. (10) to Eq. (11) in Section 1 of this chapter.

With the notation

$$G = -\frac{9\alpha \bar{f}^2 d^2 \rho_0 H}{16 m^2 p_5} \quad \text{and} \quad K_4 = 1 + \frac{3\bar{f} f d^2}{\sigma p_5^2 4 g m^2}$$

the prediction equation evolves as

$$\frac{\partial}{\partial t}\left(\bar{h} - K_4 h + J(\varphi) + G\right) + \underset{\sim}{V}\cdot\underset{\sim}{\nabla}\left(\bar{h} - K_4 h + J(\varphi) + G\right) = 0, \qquad (18)$$

or, in Jacobian form,

$$\frac{\partial}{\partial t}\left(\bar{h} - K_4 h + J(\varphi) + G\right) + \frac{g}{f} J\left(z, \bar{h} - K_4 h + J(\varphi) + G\right) = 0. \qquad (19)$$

Due to the failure of the 500-mb model to produce an acceptable prognosis, no attempt was made to test Eq. (19). Rather, a different develop-

ment was attempted in which the assumption $\underset{\sim}{V}_s = a\underset{\sim}{V}$ was not necessary, as it is believed that this assumption was the major cause of failure. The new development is presented in Chap. II.

CHAPTER II

SECOND PREDICTION MODEL

This model is designed to be applied in conjunction with a separate 500-mb prognosis, such prognosis to be made by any method the user's experience deems the most accurate. Fjortoft's method [1] is suggested. The development herein parallels that of Reed [4].

1. Development of the prediction equation.

The vertical velocity distribution of Eq. (1) is also assumed for this model. Differentiating (1) with respect to pressure yields

$$\frac{\partial \omega}{\partial p} = -\frac{K g \rho_0}{p_0}\left(\underset{\sim}{V}_s \cdot \underset{\sim}{\nabla} H\right) - 2\omega_m \frac{p - p_5}{(p_0 - p_5)^2} \quad , \tag{20}$$

and evaluation at 1000mbs gives

$$\left.\frac{\partial \omega}{\partial p}\right)_{p_0} = -\frac{K g \rho_0}{p_0}\left(\underset{\sim}{V}_s \cdot \underset{\sim}{\nabla} H\right) - \frac{2\omega_m}{p_5} \quad . \tag{21}$$

Assuming that temperature changes are adiabatic, the following form of the adiabatic thermal equation is employed:

$$\frac{\partial}{\partial t}\left(\frac{\partial z}{\partial p}\right) + \underset{\sim}{V} \cdot \underset{\sim}{\nabla} \frac{\partial z}{\partial p} + \omega \sigma = 0 \quad . \tag{22}$$

By integration from p_0 to p_5, (22) becomes

$$\frac{\partial h}{\partial t} + \underset{\sim}{V}_s \cdot \underset{\sim}{\nabla} h = \sigma \int_{p_5}^{p_0} \omega \, dp \quad . \tag{23}$$

The surface wind may be used for the advection in lieu of a suitable mean wind for the layer by considering the wind hodograph to be linear and the thermal wind relationship to hold, i.e. :

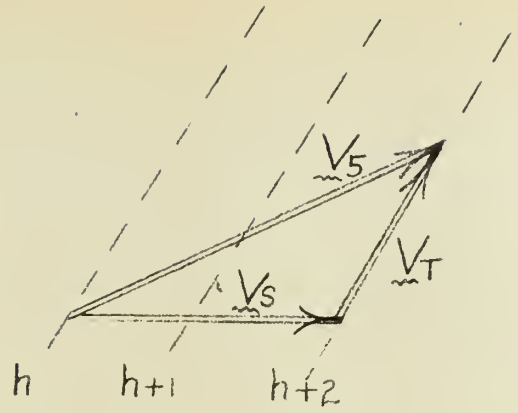

Evaluating the right side of (23) by use of (1) leads to

$$\sigma\int_{p_5}^{p_0}\omega\,dp = -\sigma K g \rho_0 (\underset{\sim}{V}_s\cdot\underset{\sim}{\nabla}H)\frac{p_0}{p_5}\int_{p_5}^{p_0}dp + \sigma\omega_m\int_{p_5}^{p_0}\left[1-\left(\frac{p-p_5}{p_0-p_5}\right)^2\right]dp\ .$$

Performing indicated integration, and noting that $p_0 = 2p_5$, gives

$$\sigma\int_{p_5}^{p_0}\omega\,dp = -\sigma K g \rho_0 (\underset{\sim}{V}_s\cdot\underset{\sim}{\nabla}H)\left[\frac{p^2}{2}\right]_{p_5}^{2p_5} + \sigma\omega_m\left[p-\frac{(p-p_5)^3}{3(p_0-p_5)^2}\right]_{p_5}^{2p_5},$$

which finally reduces to

$$\sigma\int_{p_5}^{p_0}\omega\,dp = -\frac{3}{4}\sigma K g \rho_0 (\underset{\sim}{V}_s\cdot\underset{\sim}{\nabla}H)p_5 + \frac{2}{3}\sigma p_5\omega_m\ . \qquad (24)$$

Substituting from Eq. (24) into Eq. (23) produces

$$\frac{\partial h}{\partial t} + \underset{\sim}{V}_s\cdot\underset{\sim}{\nabla}h + \frac{3}{4}\sigma K g \rho_0 (\underset{\sim}{V}_s\cdot\underset{\sim}{\nabla}H)p_5 = \frac{2}{3}\sigma p_5\omega_m\ . \qquad (25)$$

Evaluating Eq. (4) at p_0 yields

$$\frac{\partial \vartheta_0}{\partial t} + \underset{\sim}{V}_s\cdot\underset{\sim}{\nabla}(\vartheta_0+f) = f\left.\frac{\partial\omega}{\partial p}\right)_{p_0}\ , \qquad (26)$$

assuming that $\underset{\sim}{V}_s = \underset{\sim}{V}_o$. This assumption is used throughout this development. Combining (26) and (21) produces

$$\frac{\partial \zeta_o}{\partial t} + \underset{\sim}{V}_s \cdot \underset{\sim}{\nabla}(\zeta_o + f) = -\frac{fKg\rho_o}{p_o}(\underset{\sim}{V}_s \cdot \underset{\sim}{\nabla} H) - \frac{2f\omega_m}{p_5} \quad . \tag{27}$$

Multiplying (25) by factor $3f/\sigma p_5^2$ gives

$$\frac{2f\omega_m}{p_5} = \frac{3f}{\sigma p_5^2}\left[\frac{\partial h}{\partial t} + \underset{\sim}{V}_s \cdot \underset{\sim}{\nabla} h + \frac{3}{4}\sigma Kg\rho_o(\underset{\sim}{V}_s \cdot \underset{\sim}{\nabla} H)p_5\right] , \tag{28}$$

which, upon substituing in (27), yields

$$\frac{\partial \zeta_o}{\partial t} + \underset{\sim}{V}_s \cdot \underset{\sim}{\nabla}(\zeta_o + f) = -\frac{fKg\rho_o}{p_o}(\underset{\sim}{V}_s \cdot \underset{\sim}{\nabla} H)$$

$$-\frac{3f}{\sigma p_5^2}\left[\frac{\partial h}{\partial t} + \underset{\sim}{V}_s \cdot \underset{\sim}{\nabla} h + \frac{3}{4}\sigma Kg\rho_o(\underset{\sim}{V}_s \cdot \underset{\sim}{\nabla} H)p_5\right] . \tag{29}$$

Collecting advective terms and time derivatives, and again noting that $p_o = 2p_5$, (29) may be written

$$\frac{\partial}{\partial t}\left(\zeta_o + \frac{3f}{\sigma p_5^2} h\right) = -\underset{\sim}{V}_s \cdot \underset{\sim}{\nabla}\left[\zeta_o + \frac{3f}{\sigma p_5^2} h + f + \frac{11Kg\bar{f}\rho_o}{2p_o} H\right] . \tag{30}$$

Making the geostrophic approximation for ζ_o leads to

$$\frac{\partial}{\partial t}\left[\frac{4m^2 g}{fd^2}(\bar{z}_o - z_o) + \frac{3f}{\sigma p_5^2} h\right] =$$

$$-\underset{\sim}{V}_s \cdot \underset{\sim}{\nabla}\left[\frac{4m^2 g}{fd^2}(\bar{z}_o - z_o) + \frac{3f}{\sigma p_5^2} h + f + \frac{11Kg\bar{f}\rho_o}{2p_o} H\right] , \tag{31}$$

which, after multiplying by factor $fd^2/4m^2 g$, yields

$$\frac{\partial}{\partial t}\left[(\bar{Z}_o - Z_o) + \frac{3f^2d^2}{4m^2g\sigma p_5^2}h\right] =$$

$$-\underset{\sim}{V_s}\cdot\nabla\left[(\bar{Z}_o - Z_o) + \frac{3f^2d^2}{4m^2g\sigma p_5^2}h + J(\varphi) + \frac{11K\bar{f}^2d^2\rho_o}{8m^2p_o}H\right], \quad (32)$$

where

$$J(\varphi) = \int_o^{\varphi} \frac{\Omega^2 d^2 \sin\varphi\cos\varphi}{m^2 g}\, d\varphi$$

following Fjortoft [1]. With the notation

$$F = \frac{11K\bar{f}^2d^2\rho_o}{8m^2p_o} \qquad \text{and} \qquad C = \frac{3f^2d^2}{4m^2g\sigma p_5^2},$$

(32) may be written

$$\frac{\partial}{\partial t}\left[\bar{Z}_o - Z_o + Ch + J(\varphi) + F\right] = \underset{\sim}{V_s}\cdot\underset{\sim}{\nabla}\left[\bar{Z}_o - Z_o + Ch + J(\varphi) + F\right]$$

as $J(\varphi)$ and F are invariant with time. This is the prediction equation, which may be written in Jacobian form as

$$\frac{\partial}{\partial t}\left[\bar{Z}_o - Z_o + Ch + J(\varphi) + F\right] = -\frac{g}{f}J\left[Z_o, \bar{Z}_o - Z_o + Ch + J(\varphi) + F\right]. \quad (33)$$

However, if (33) were to be used in prognosis, the advection would be accomplished with the current 1000-mb chart, which may vary considerably over a prognostic period of 12 or 24 hours. In order to arrive at a more conservative advective field, the Jacobian identity

$$J(X, Y) \equiv J(X+Y, Y)$$

may be employed. Applying this to (33) leads to

$$\frac{\partial}{\partial \tau}\left[\bar{Z}_o - Z_o + Ch + J(\varphi) + F\right] =$$

$$-\frac{g}{f}J\left[\bar{Z}_o + Ch + J(\varphi) + F,\ \bar{Z}_o - Z_o + Ch + J(\varphi) + F\right], \quad (34)$$

which accomplishes the advection with a more stable field than Z_o.

To recover height changes, the local change in the advected quantity over the prognostic period may be written

$$\Delta\left[\overline{Z}_o - Z_o + Ch + J(\varphi) + F\right] = -A \quad ,$$

or

$$\Delta\left[\overline{Z}_o - Z_o + Ch\right] = -A \quad , \tag{35}$$

as F and $J(\varphi)$ are invariant with time. With the relationship $h = Z_5 - Z_o$, (35) may be written

$$\Delta\left[\overline{Z}_o - Z_o + CZ_5 - C Z_o\right] = -A \tag{36}$$

Solving for ΔZ_o yields

$$\Delta Z_o = \frac{1}{C+1}\left[A + \Delta\overline{Z}_o + C\,\Delta Z_5\right] \tag{37}$$

Utilizing Fjortoft's method [1] to evaluate $\Delta\overline{Z}_o$ gives

$$\Delta\overline{Z}_o \doteq \frac{2}{C+1}\left[\overline{A} + C\,\Delta\overline{Z}_5\right] \tag{38}$$

Substituting (38) into (37) yields

$$\Delta Z_o \doteq \frac{1}{C+1}\left[A + \frac{2}{C+1}\,\overline{A}\right] + \frac{C}{C+1}\,\Delta Z_5 \tag{39}$$

Testing indicated that $A \doteq 2\overline{A}$, so (39) is simplified to

$$\Delta Z_o = A\left[\frac{1}{C+1} + \frac{1}{(C+1)^2}\right] + \frac{C}{C+1}\,\Delta Z_5 \tag{40}$$

which further reduces to

$$\Delta Z_o \doteq 0.8\,A + 0.5\,\Delta Z_5 \tag{41}$$

For simplicity of application, Eq. (41) was further simplified to

$$\Delta Z_0 = A + 0.5\Delta Z_5 \quad , \qquad (42)$$

which was the equation utilized. However, testing indicated that Eq. (41) may have given better results than the simplified form of Eq. (42).

2. Testing of the prediction equation.

The prognostic period of 12 hours was chosen to test the prediction equation. Four successive 12-hr intervals were prognosticated starting with the 0030Z chart of 14 November, 1955. Since the purpose of this paper is to attempt improvement in graphical prognosis by the inclusion of terrain effects, the prediction equation was applied in two different forms. First, a prognosis was made applying Eq. (34), and a second prognosis using

$$\frac{\partial}{\partial t}\left[\bar{Z}_0 - Z_0 + Ch + J(\varphi)\right] = -\frac{g}{f} J\left[\bar{Z}_0 + Ch + J(\varphi), \bar{Z}_0 - Z_0 + Ch + J(\varphi)\right], \qquad (43)$$

which is simply (34) neglecting vertical motion induced by terrain. With minor differences, Eq. (43) is the prediction equation derived by Reed [4].

In applying (34), the following steps were carried out:

(a) The current $\bar{Z}_0$ chart was constructed by conventional graphical methods, using a grid distance of 600Km.

(b) The current thickness chart was multiplied by the constant C and added to the $\bar{Z}_0$ chart. In practice, using a value of 0.75 for C in this step was found to give better results than the derived value of 0.9, and consequently this value was used.

(c) Considering $k = 1$, the coefficient of H in the quantity F was evaluated to be 7.35×10^{-2}. A terrain contour chart was multiplied by this factor to produce the quantity F, and isolines of F were added to contours of $J(\varphi)$. The chart of $F + J(\varphi)$ (Fig. 2) was added to contours

Fig. 2

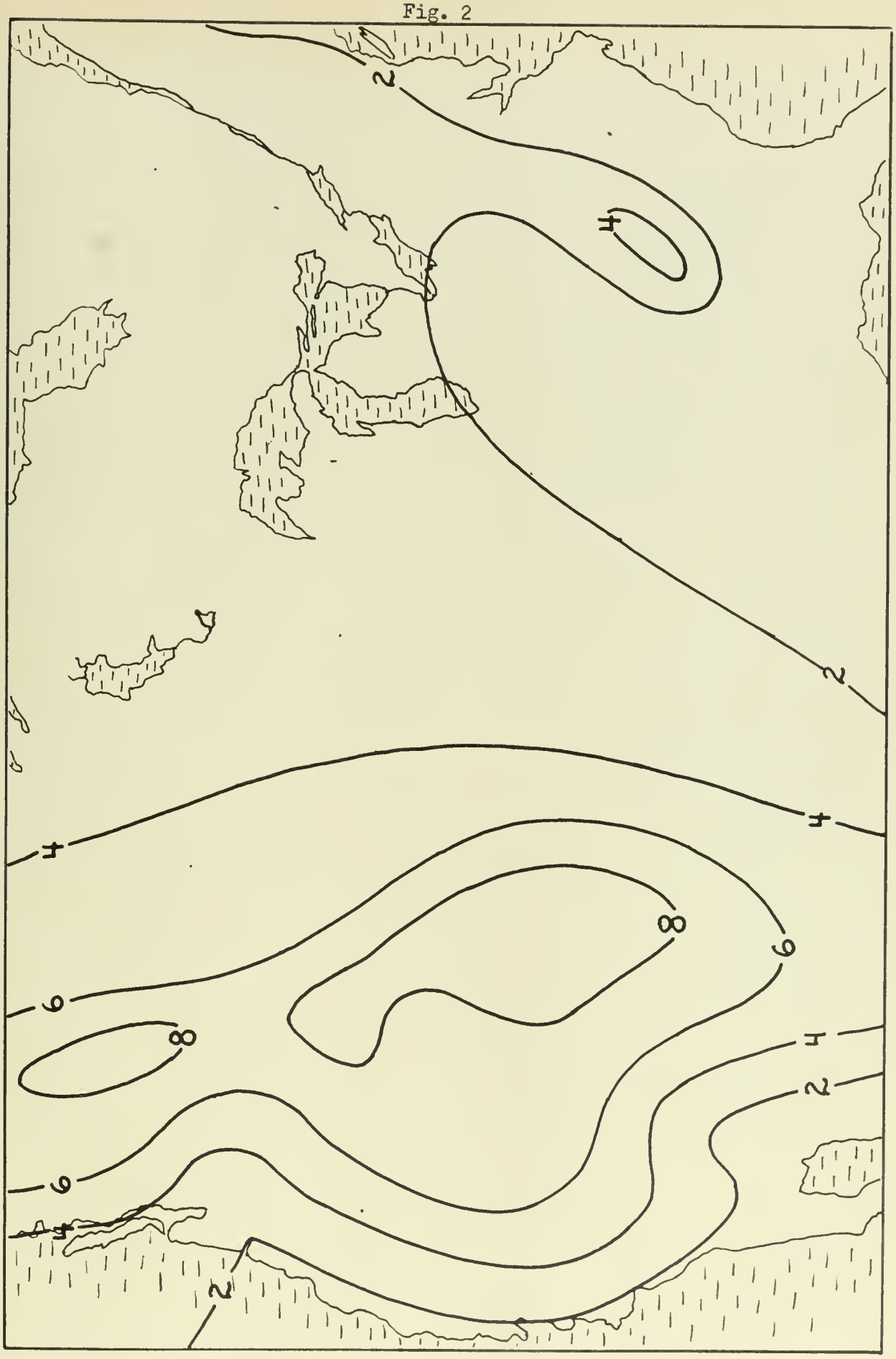

produced in step (b) to produce the advective field $(\overline{Z}_o + Ch + J(\varphi) + F)$.

(d) The current Z_o chart was graphically subtracted from the advective field to produce the conserved quantity $(\overline{Z}_o - Z_o + Ch + J(\varphi) + F)$.

(e) Charts (c) and (d) were superimposed, and isolines of the conserved quantity advected geostrophically with the advective field for the prognostic period of 12 hours. A difficulty arose in the advection process along the west coast of the United States and Canada due to the extreme gradients of the advective field caused by the high coastal mountain ranges. It was reasoned that where the terrain gradient was very large the horizontal wind would not be fully translated into upslope motion, and therefore result in lesser vertical velocities. Thus the scalar multiplier k in Eq. (32) may be appreciably less than unity in regions of such strong terrain gradients. The amount of reduction of k was determined by cases tested. This reduction factor may be taken into account by appropriately reducing the gradients of F where the gradient is very large. The final form of F is given in Fig. 2.

(f) The advected isolines of $(\overline{Z}_o - Z_o + Ch + J(\varphi) + F)$ were subtracted graphically from the initial isolines of the same quantity to produce isolines of A.

(g) Half of the 12-hr 500-mb height change was added graphically to A to produce the ΔZ_o chart. In practice, any suitable method of prognosticating the 500-mb chart could be employed, but for this test the actual 500-mb height change was used in order that the prediction equations, Eqs. (34) and (43), might be more objectively compared.

In applying Eq. (43), the steps were identical to the above, with the exception that in step (c) only the contours of $J(\varphi)$ were added.

The results of the above tests are displayed in Table 1, which com-

TABLE 1

		1	2	3	4
Correlation coefficient	A	0.832	0.847	0.710	0.790
	B	0.707	0.673	0.580	0.630
	C	0.844	0.851	0.790	0.812
	D	0.866	0.870	0.924	0.848
Root-mean-square error	A	94ft	116ft	103ft	99ft
	B	115ft	172ft	169ft	160ft
	C	85ft	102ft	88ft	89ft
	D	67ft	74ft	53ft	69ft

A : Prognostication including terrain factor; computations for area west of 96W, i.e., Rocky Mountain area.

B : Prognostication excluding terrain factor; computations for area west of 96W.

C : Prognostication including terrain factor; computations for entire area covered by grid.

D : Prognostication including terrain factor; computations for area east of 96W.

1 : 12-hr prognostic period commencing 0030Z 14 November, 1955.

2 : " " " " 1230Z " " " .

3 : " " " " 0030Z 15 " " .

4 : " " " " 1230Z " " " .

pares height changes as prognosticated by the two methods to the observed height changes. The statistical parameters were computed using a 48 point square grid, which enclosed the area bounded by points 28N, 124W; 55N, 136W; 53N, 65W; and 27N, 79W. Figs. 3, 4, and 5 illustrate height changes for the period 1230Z 15 November to 0030Z 16 November, 1955. Fig. 3 shows observed height changes, Fig. 4 the height changes as prognosticated by Eq. (34), and Fig. 5 the height changes as prognosticated by Eq. (43). The grid encompasses an area slightly larger than the above illustrations.

3. Conclusions.

The inclusion of the terrain factor in this model results in materially improved prognoses.

However, the process of making a prognosis by this method is rather lengthy, and whereas the inclusion of the terrain factor into the prediction equation adds no more steps to the routine, (F may be combined with $J(\varphi)$ on a permanent chart and used for each prognosis), the advective procedure is much more delicate. The advective field has areas of very strong gradient with the isolines of the conserved quantity closely packed and almost parallel to the advective field. Consequently considerable care must be taken to insure accurate advection.

In constructing the contours of F, terrain irregularities were smoothed to some extent. Some smoothing is mandatory, as a minutely accurate F chart is not reasonable to use when considering large scale flow. Also, it is evident that the smoother the F chart, the easier the graphical constructions will be. Further testing might indicate an optimum balance between detail of the terrain features and representation for large scale flow.

As noted in Sect. 2, a value of 0.75 was used as a multiplier of h

Fig. 3

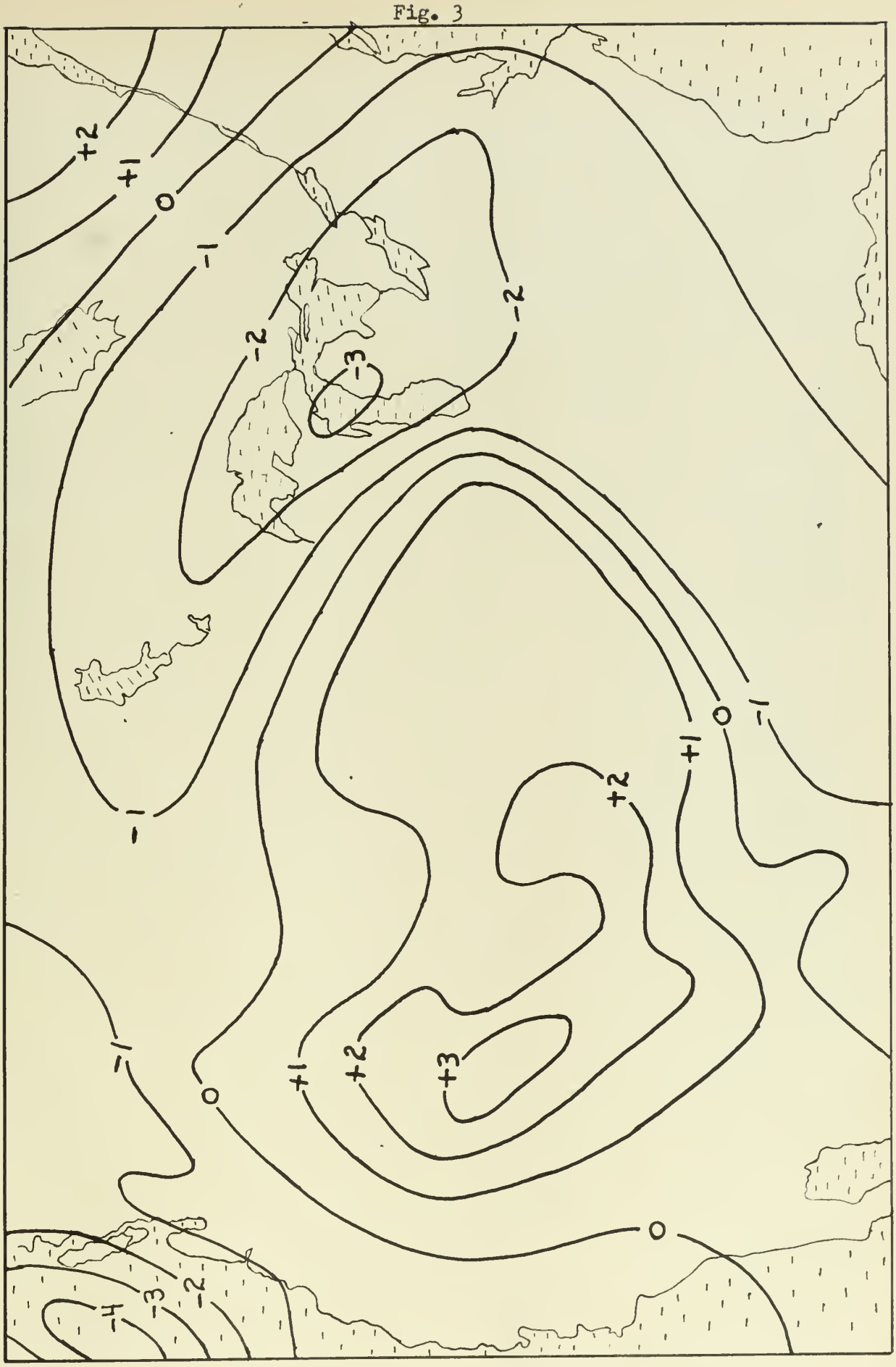

Fig. 4

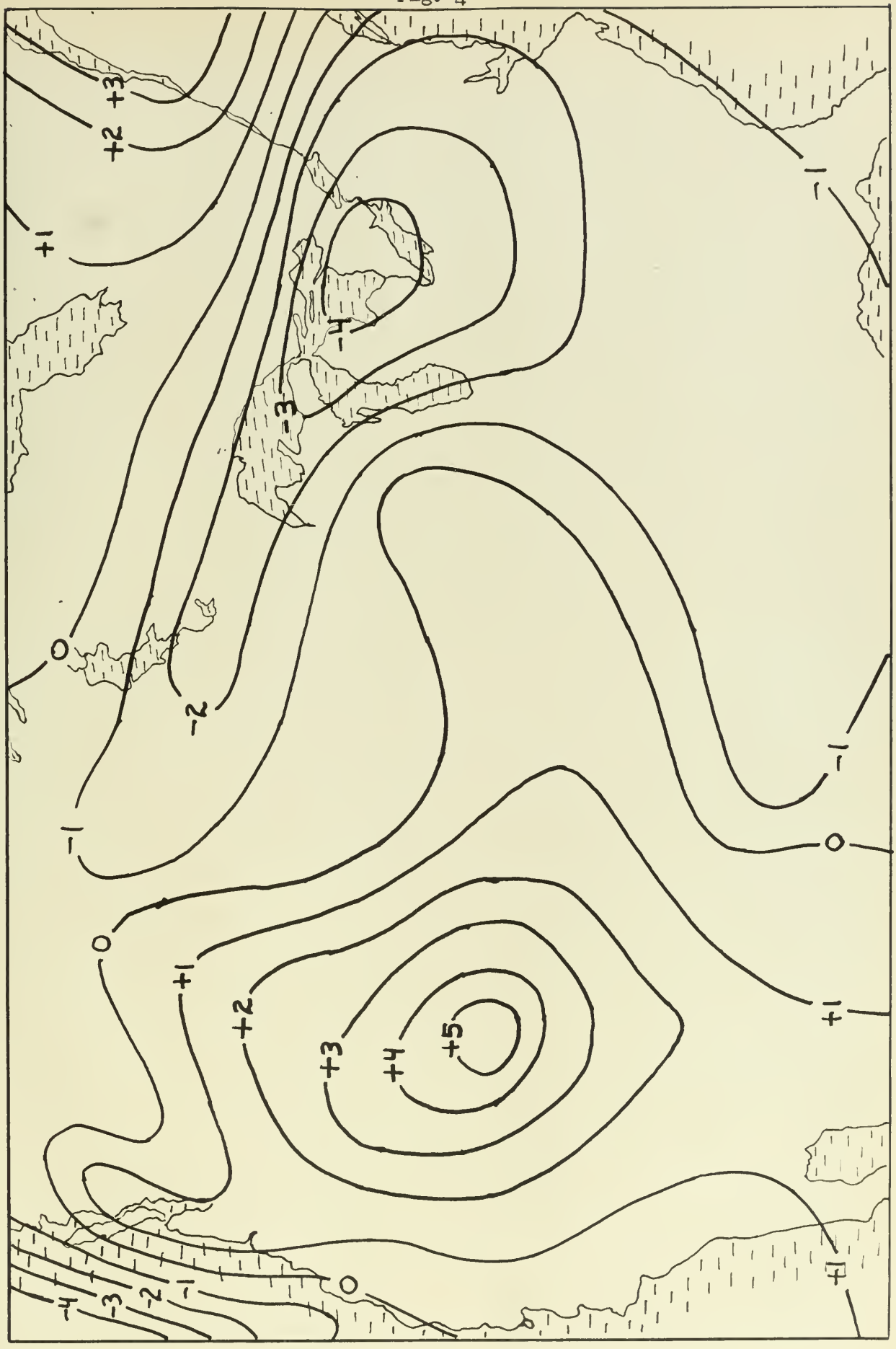

Fig. 5

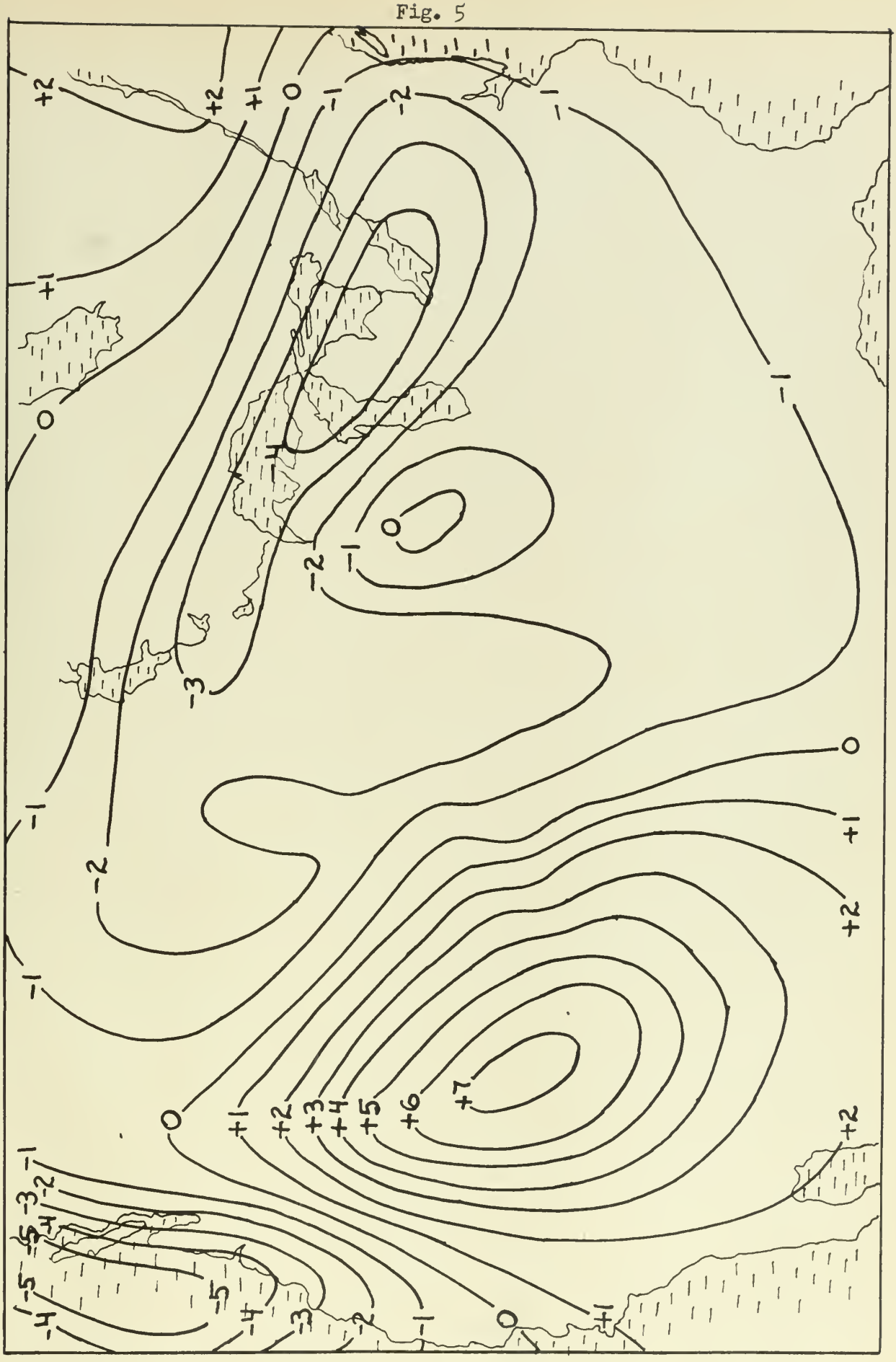

in producing the advective field rather than the derived value of 0.9. More extensive testing would doubtless indicate the optimum value of this multiplier. Reed [4] found that a value of 0.5 gave good results in the three cases tested with his model.

BIBLIOGRAPHY

1. Fjortoft, R., 1952 : On a Numerical Method of Integrating the Barotropic Vorticity Equation. Tellus, 4, 179-194.

2. Air Weather Service, 1955 : Fjortoft's Graphical Method for Preparing 24-hr 500-mb Prognostic Charts. (Tech. Rep. 105-131), Washington, Military Air Transport Service, 11 pp.

3. Estoque, M. A. , 1956 : A Prediction Model for Cyclone Development Integrated by Fjortoft's Method. Journal of Meteorology, 13, 195-202.

4. Reed, R. J., 1957 : A Graphical Method for Preparing 1000-mb Prognostic charts. Journal of Meteorology, 14, 65-70.